The conserved GTPase Gem1 regulates endoplasmic reticulum–mitochondria connections

Benoît Kornmann[a,1,2], Christof Osman[a], and Peter Walter[a,b,2]

[a]Department of Biochemistry and Biophysics and [b]Howard Hughes Medical Institute, University of California, San Francisco, CA 94158

Contributed by Peter Walter, July 15, 2011 (sent for review June 15, 2011)

Mitochondria are connected to the endoplasmic reticulum (ER) through specialized protein complexes. We recently identified the ER–mitochondria encounter structure (ERMES) tethering complex, which plays a role in phospholipid exchange between the two organelles. ERMES also has been implicated in the coordination of mitochondrial protein import, mitochondrial DNA replication, and mitochondrial dynamics, suggesting that these interorganelle contact sites play central regulatory roles in coordinating various aspects of the physiology of the two organelles. Here we purified ERMES complexes and identified the Ca^{2+}-binding Miro GTPase Gem1 as an integral component of ERMES. Gem1 regulates the number and size of the ERMES complexes. In vivo, association of Gem1 to ERMES required the first of Gem1's two GTPase domains and the first of its two functional Ca^{2+}-binding domains. In contrast, Gem1's second GTPase domain was required for proper ERMES function in phospholipid exchange. Our results suggest that ERMES is not a passive conduit for interorganellar lipid exchange, but that it can be regulated in response to physiological needs. Furthermore, we provide evidence that the metazoan Gem1 ortholog Miro-1 localizes to sites of ER–mitochondrial contact, suggesting that some of the features ascribed to Gem1 may be evolutionarily conserved.

membranes | TAP-purification | EF hand | calcium | yeast

The structural and functional coordination of intracellular organelles is critical to maintain homeostasis. The endoplasmic reticulum (ER) and mitochondria have recently emerged as a paradigm for interorganelle communication (1–3). Both organelles are physically tethered by protein complexes, which establish a spatial proximity allowing privileged exchange of metabolites and information. Membrane lipids synthesized in the ER are transported to both the inner mitochondrial membrane and the outer mitochondrial membrane (OMM) using such interorganelle contact sites as exchange platforms. Similarly, Ca^{2+} released by the ER upon stimulation of the inositol-3-phosphate receptor is transferred to the mitochondrial matrix, perhaps exploiting high local concentrations maintained by ultrastructural boundaries established at ER–mitochondrial contact sites akin to boundaries defining synaptic spaces between neurons and other cells (1).

We recently identified ER–mitochondria encounter structures (ERMESs) in the budding yeast *Saccharomyces cerevisiae* (4). ERMES constitutes a molecular zipper that links the ER and OMM. The core building block of ERMES is a heterotetrameric protein complex composed of Mmm1, an ER-resident integral membrane protein; Mdm12, a cytosolic protein; Mdm34, a putative OMM protein; and Mdm10, an integral β-barrel OMM protein (Fig. S1*B*). In cells, these protein complexes are arranged in larger assemblies, visible microscopically as one to five discrete puncta per cell at the ER–mitochondria interface.

Experimentally, ERMES was shown to be important for proper phospholipid exchange between the two organelles (4). Lipid transport may be mediated by SMP domains, present in Mmm1, Mdm12, and Mdm34. SMP domains are homologous to the structurally well-characterized TULIP domain present in many lipid-binding proteins (5). A number of TULIP domains have been crystallized. The oblong domains contain longitudinally extended promiscuous hydrophobic pockets, in which the hydrophobic moieties of different lipids can bind. In ERMES, the three SMP domains may be aligned to provide a hydrophobic slide bridging the aqueous gap between the ER and OMM to allow interorganellar lipid exchange (5).

ERMES has been implicated in biological roles extending beyond lipid exchange. For instance, ERMESs colocalize with actively replicating nucleoids, indicating that ERMES may be involved in the regulation of mitochondrial DNA replication (6, 7). Furthermore, ERMES may play a role in mitochondrial protein import. Mdm10 is a component of both ERMES and of the sorting and assembly machinery (SAM) that assembles membrane β-barrel proteins in the OMM (8). Whereas the SAM complex assembles different β-barrel substrates, Mdm10 associates with SAM as an accessory factor that specifically assists the assembly of Tom40, the central translocase of the TOM (translocase of the OMM) complex. Both absence and overexpression of Mdm10 is detrimental to Tom40 biogenesis, suggesting that partitioning of Mdm10 between ERMES and SAM complexes could serve regulatory roles in mitochondrial biogenesis.

Finally, ERMES has been proposed to play a role in the association between mitochondria and the actin cytoskeleton. Mitochondria of ERMES mutants have an aberrant morphology and motility and are incapable of binding actin in vitro (9).

These diverse functions place the ERMES complex at the crossroad of many central pathways of mitochondrial biology. However, how cellular signals are integrated by ERMES and how such integration might serve to regulate mitochondrial biology remain unclear. Here we identify the Ca^{2+}-binding Miro (mitochondrial rho-like) GTPase Gem1 as an integral regulatory component of the ERMES complex. Gem1 contains two GTPases and two Ca^{2+}-binding EF hand domains. Most regulatory GTPases bind to their cognate effectors differentially according to their guanine-nucleotide binding status (10). Thus, signaling cues might be integrated by the EF hands, and the GTPase domains may cycle between GTP-bound and GDP-bound forms to adopt different regulatory states. As such, Gem1 exhibits hallmarks of a regulatory protein.

Results

We purified the ERMES complex from digitonin-solubilized whole-cell extracts of strains bearing functional, C-terminally tandem affinity purification (TAP)-tagged versions of either Mmm1 or Mdm34. Purified complexes were resolved on SDS/PAGE, stained with colloidal Coomassie blue, and subjected to liquid chromatography–tandem mass spectrometry. Both tagged

Author contributions: B.K., C.O., and P.W. designed research; B.K. and C.O. performed research; B.K., C.O., and P.W. analyzed data; and B.K., C.O., and P.W. wrote the paper.

The authors declare no conflict of interest.

Freely available online through the PNAS open access option.

[1]Present address: ETH Zürich, Institute of Biochemistry, Zürich CH-8093, Switzerland.

[2]To whom correspondence may be addressed. E-mail: benoit.kornmann@bc.biol.ethz.ch or walter@cgl.ucsf.edu.

This article contains supporting information online at www.pnas.org/lookup/suppl/doi:10.1073/pnas.1111314108/-/DCSupplemental.

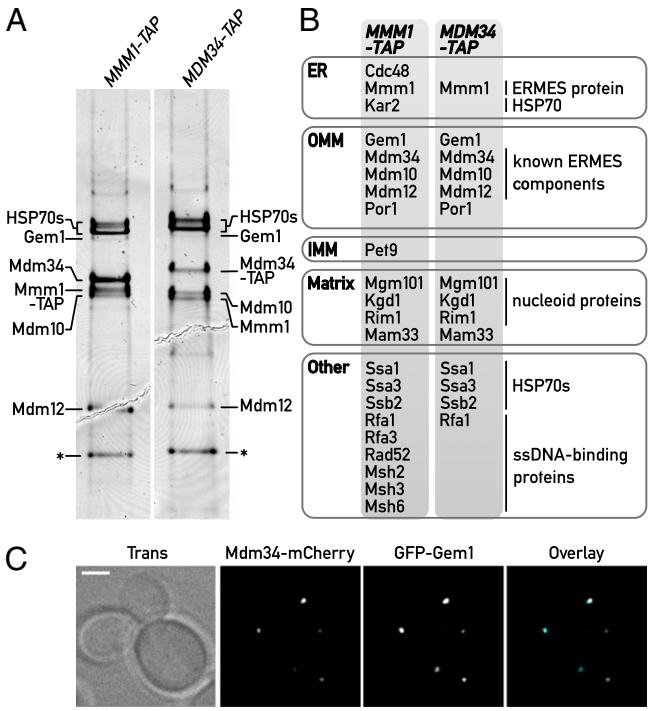

Fig. 1. (*A*) Silver-stained gel of protein complexes isolated by affinity purification of Mmm1-TAP (*Left*) and Mdm34-TAP (*Right*). Asterisks indicate an abundant protein that has not been identified. (*B*) Identity and subcellular localization of proteins identified by LC-MS/MS of the complexes shown in *A*. (*C*) Gem1 localizes to ER–mitochondria interfaces. Deconvoluted Z-stack of a live yeast strain harboring *MDM34-mCherry* and *GFP-GEM1* fusion alleles. Mdm34-mCherry displays the expected punctate pattern (*Middle Left*). GFP-Gem1 localizes to foci (*Middle Right*) that colocalize with Mdm34-mCherry (*Right*; red, Mdm34-mCherry; cyan, GFP-Gem1). (Scale bar: 2 μm.)

proteins pulled down a similar set of proteins (Fig. 1 *A* and *B*), including all other previously identified ERMES subunits. In contrast to previous reports (11), these results indicate that Mmm1 and Mdm34 are physically present in the same complexes.

Mass spectrometry identified several ERMES-associated proteins listed in Fig. 1*B*. Among these, we identified the Ca^{2+}-binding Miro GTPase Gem1 as a binding partner of the ERMES complex. Miro GTPases are conserved proteins that play a role in mitochondrial movement and inheritance. In organisms in which mitochondrial movements are microtubule-driven, Miro GTPases anchor mitochondria directly to the kinesin heavy chain (12, 13). In yeast, where mitochondrial movement is actin-based, Gem1 is required for mitochondrial morphology maintenance and inheritance, but the underlying molecular mechanisms remain unknown (14, 15).

To confirm the interaction between the ERMES complex and Gem1 with an independent assay, we determined the subcellular localization of an N-terminally GFP-tagged Gem1 fusion protein by fluorescence microscopy. This fusion protein construct is at least partially functional, given that it was previously shown to complement a growth defect of *gem1*Δ cells, albeit not to the same degree as WT *GEM1* (14). When visualized by fluorescent microscopy, GFP-Gem1 colocalized with Mdm34-mCherry in a few foci per cell, which is the characteristic localization pattern observed for ERMESs (Fig. 1*C*; also see Fig. 2*D*). The colocalization suggests that most, if not all, Gem1 functions at ERMES.

Akin to Mmm1, Mdm12, Mdm10, and Mdm34, Gem1 could be a structural component of ERMES required for the establishment of ER–mitochondria interfaces. Alternatively, Gem1 could act as a regulatory subunit of the ERMES complex, as suggested by its GTPase and Ca^{2+}-binding domains.

To distinguish between these models, we asked whether ERMES foci are observed in the absence of Gem1. As shown in Fig. 2*A*, this was the case; Mdm34-GFP fusion protein localized to ERMES foci in *gem1Δ* cells (Fig. 2*A*), in contrast to the deletions of other ERMES components in which ERMES foci disappear (4, 9). These foci represent bona fide ER–mitochondria contact sites, because the formation of such foci requires the ER protein Mmm1 (4, 9, 11). Thus, ERMESs form in the absence of Gem1. But quantification of both the size and number of ERMES foci revealed that in *gem1Δ* cells, the fluorescent signal of Mdm34-GFP was distributed into fewer and larger foci (Fig. 2 *A* and *B*), whereas the total amount of Mdm34-GFP was unchanged (Fig. 2*C*). This indicates that *GEM1* deletion results in a redistribution of ERMES complexes and suggests that Gem1 regulates ERMES organization.

To assess the putative role of Gem1's GTPase domains as molecular switches, we next used Gem1 mutants predicted to lock each GTPase into a functionally discrete conformation (14, 16). We assessed whether these mutations affect the localization of Gem1 to ERMES foci by expressing GFP-Gem1 mutant constructs over a WT copy of Gem1. Although the in vivo activity of the GFP-Gem1 fusion protein is impaired partially, our data in Fig. 1*C* show that the mechanism(s) of association with ERMES is operational in this fusion protein. It thus can be used as a proxy for assessing Gem1 recruitment to ERMES in different mutant backgrounds.

Homology to the well-characterized GTPase $p21^{Ras}$ predicts that the conserved lysine K18 of the first GTPase domain of Gem1 and K461 of the second domain, as well as serine S19 and S462, are important for nucleotide hydrolysis. Mutations of the corresponding residues in $p21^{Ras}$ (K16A and S17N) abrogate the catalytic activity and impair nucleotide binding (17, 18). Mutation of these residues in Gem1 was previously shown to compromise mitochondrial shape and inheritance (14, 16). We observed that GFP-Gem1(K18A) and GFP-Gem1(S19N), both bearing mutations localized to the first GTPase domain, abrogated Gem1 localization to ERMES foci (Fig. 2*D*, yellow arrowheads and Fig. 2*F*). In contrast, GFP-Gem1(K461A) and GFP-Gem1(S462N), bearing mutations in the second GTPase domain, localized properly to ERMES foci. Identical results were obtained with cells expressing the variants Gem1(K461A) and Gem1(S462N) in *gem1Δ* cells, ruling out the possibility that the presence of WT Gem1 masks colocalization defects of the mutant Gem1 variants (Fig. S2).

A mutation in the conserved threonine T35 of Ras has been shown to abrogate effector binding (19). Corresponding mutations in Gem1 (T33A and T480A) did not disturb Gem1 subcellular localization (Fig. 2*D*). Consistent with this observation, such mutants were previously shown to have a marginal impact on mitochondrial morphology (14).

We also generated mutants of Gem1's EF hands. A conserved glutamate residue of the EF hand motif is crucial for Ca^{2+} coordination, and substitution of this residue to lysine abrogates Ca^{2+} binding (16). We introduced this mutation into the first (E225K), second (E354K), or both EF hands. Mutating the first EF hand had a strong effect on Gem1 localization to ERMES foci, indistinguishable from that observed after mutating the first GTPase domain (Fig. 2 *D*–*F*). Mutating the second EF hand had no effect on localization and only a marginal effect on mitochondrial morphology (14). Where observed, the absence of mutant Gem1 proteins from ERMES foci reflects a localization defect, because all proteins were expressed at comparable levels (Fig. 2*E*). This is in contrast to previous reports showing destabilization of Gem1 variants harboring the E225K mutation (16). We do not know the reasons for this discrepancy. It may arise from the fact that we expressed the GFP-Gem1 fusion protein and mutant versions thereof over a WT copy of Gem1, which might have stabilized the GFP-Gem1 mutant proteins.

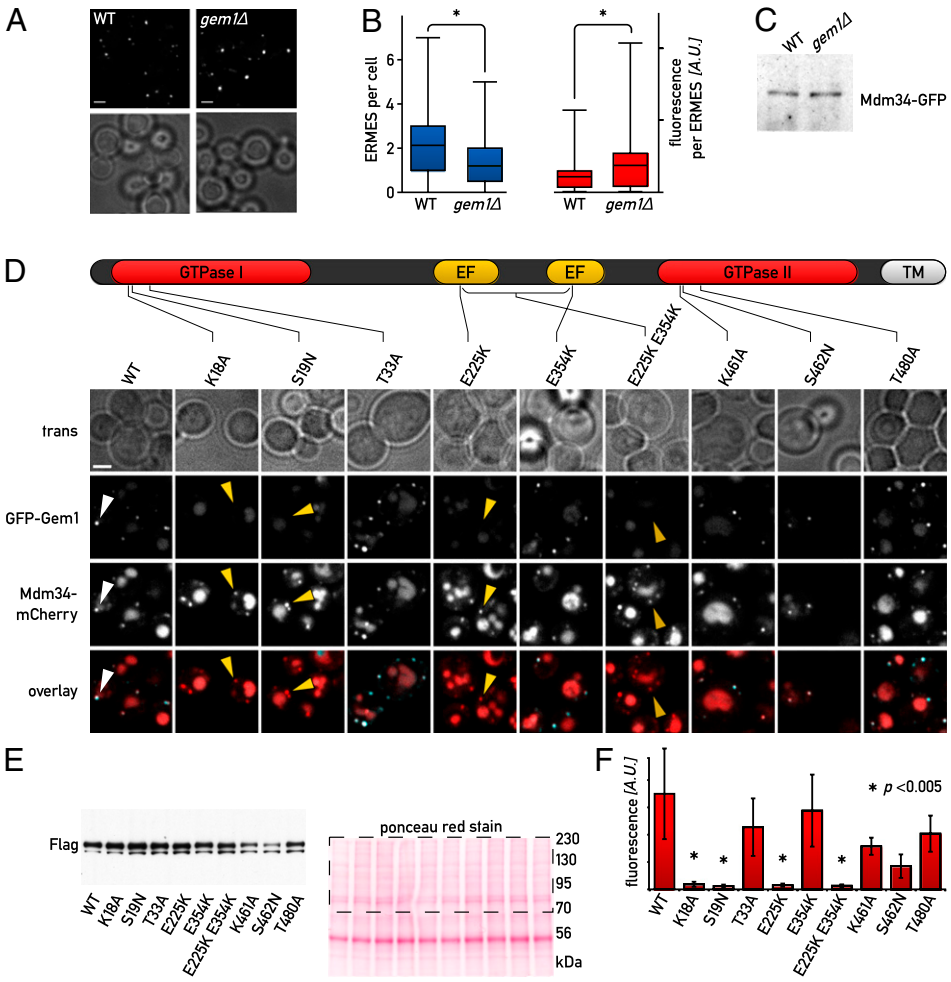

Fig. 2. (*A*) Gem1 is not required for ERMES assembly. Mdm34-GFP assembles into foci in the presence (*Upper*) or absence (*Lower*) of Gem1, indicating that the ER–mitochondria interface is intact in these cells. (Scale bar: 2 μm.) (*B*) Gem1 regulates ERMES size and number. Images of Mdm34-GFP were quantified, and the average number of ERMES foci per cell (*Left*) and average fluorescence intensity of individual ERMES foci (*Right*) were plotted. Brackets represent the extreme measured values, and boxes represent the upper and lower quartiles. *$P < 10^{-10}$, two-tailed Student *t* test. WT, $n = 164$ cells; *gem1*Δ, $n = 155$ cells. (*C*) Western blot analysis using an α-GFP antibody, showing that total amounts of Mdm34-GFP are unaffected by the deletion of *GEM1*. (*D*) Nucleotide and Ca^{2+} binding are important for Gem1 localization to ERMES. Indicated mutants of Gem1 were expressed as N-terminal 2× Flag-GFP fusions under the Gem1 promoter and colocalized with Mdm34-mCherry. White arrowheads indicate Gem1-containing ERMES; yellow arrowheads indicate ERMES devoid of Gem1. (Scale bar: 2 μm.) (*E*) (*Left*) Western blot quantitation of 2× Flag-GFP-Gem1 expression shows that all variants are expressed to comparable levels. (*Right*) Ponceau red staining of the membrane used for the Western blot analyses, showing equal loading. The boxed area corresponds to the approximate location of the blot shown in the left panel. (*F*) Quantifications of Gem1 signal present in ERMES foci (*SI Appendix*). The *P* value is computed using a *t* test on $n = 6$ images each containing ~12 cells. The slightly lower levels of Gem1 localized in ERMES observed for the S462N mutant might be explained by a lower protein accumulation.

Taken together, these data suggest that the nucleotide binding status in the first GTPase domain and Ca^{2+} binding to the first EF hand influence the localization of Gem1 to ERMES foci.

Regulation of ERMES by Gem1 may be important for ERMES function in interorganelle phospholipid exchange. Cells bearing mutations in ERMES components display phenotypes related to phospholipid biosynthesis and homeostasis, such as reduced cardiolipin (CL) levels, synthetic genetic interactions with enzymes of the CL biosynthesis pathway, and an overall similarity in the pattern of genetic interaction with a mutant of the mitochondrial phosphatidylserine (PS) decarboxylase *PSD1* (4) (Fig. S1). We observed similar phenotypes in *gem1Δ* cells (4) (Fig. 3*A*). For example, we detected a strong synthetic genetic interaction between *GEM1* and the cardiolipin synthase *CRD1* with the recently discovered phosphatidylglycerol-phosphate phosphatase *GEP4*, which functions upstream of *CRD1* in CL synthesis (20), as well as with the putative phospholipase *FMP30*, which is required for normal cardiolipin level accumulation (21) (Fig. 3 *A* and *B*). The phenotypic similarity between *gem1Δ* and other ERMES mutants suggests that Gem1-dependent organization of ERMES affects phospholipid exchange between the ER and mitochondria.

In contrast to the Gem1 localization to ERMES foci shown in Fig. 2, which was affected only by mutations in the first GTPase domain, both GTPases and the first Ca^{2+}-binding domain were required for ERMES function in lipid exchange. Mutants compromised in nucleotide binding and hydrolysis in the first (K18A, S19N) and second (K461A, S462N) GTPase domains failed to rescue the synthetic lethality of a *gem1Δ gep4Δ* strain (Fig. 3*C*). Mutants of the first EF hand also did not rescue efficiently, whereas mutants in the second EF hand behaved like WT. This indicates that mutants that fail to localize at ERMES also fail to rescue the synthetic lethality of a *gem1Δ gep4Δ* strain. In addition, mutants of the second GTPase domain display the same defects

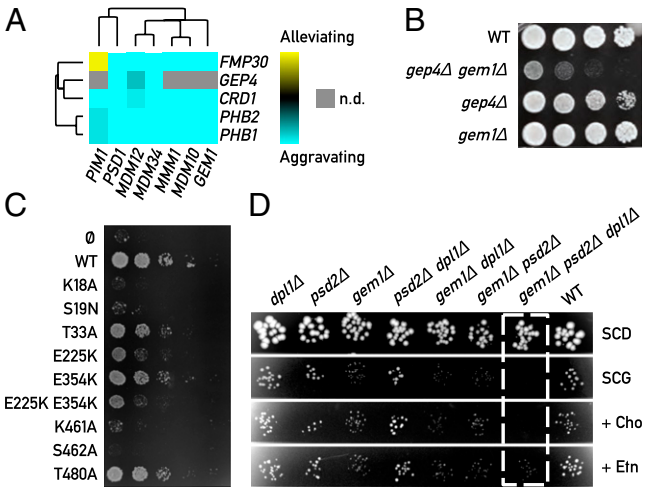

Fig. 3. (*A*) Synthetic interactions between ERMES members and the cardiolipin biosynthesis pathway. The cyan color denotes synthetic or aggravating interactions between deletions of the referred genes. The trees denote hierarchical clustering obtained comparing the patterns of synthetic interactions across the whole dataset (4). (*B*) *GEM1* displays a synthetic interaction with the PGP phosphatase *GEP4*. (*C*) A *gep4Δ gem1Δ* strain was transformed with a plasmid encoding the indicated version of Gem1 (Fig. 2*D*) and growth was assayed by spotting serial dilutions of saturated cultures on YPD plates. (*D*) Defect in the mitochondrial pathway of PE biosynthesis in the absence of Gem1. Cells display a synthetic growth defect when *GEM1* deletion is combined with deletions affecting the Golgi/vacuolar PE biosynthesis pathway (*psd2Δ*) and the Kennedy pathway of PE biosynthesis (*dpl1Δ*) on a nonfermentable carbon source (synthetic complete + glycerol, SCG). This synthetic defect can be suppressed by exogenous ethanolamine (+Etn), but not by choline (+Cho).

as the null allele, although they localize properly to ERMES as GFP fusions. This analysis suggests that the two Gem1 GTPase domains are involved in separate regulatory events: (*i*) localizing Gem1 to ERMESs (first GTPase domain) and (*ii*) once in place, controlling ERMES function (second GTPase domain).

The synthetic phenotypes observed between ERMES and CL biosynthesis mutants are likely due to a defect in PS and phosphatidylethanolamine (PE) shuttling between the ER and the mitochondria (4) during de novo phosphatidylcholine (PC) biosynthesis (Fig. S1), and can be explained by partially redundant roles of PE and CL in mitochondrial membranes (22). However, we detected no strong alterations in *gem1Δ* cells of the steady-state phopholipid levels in mitochondrial or total membrane fractions (not shown), or in the PC biosynthesis rates (Fig. S3). This discrepancy may arise from the fact that PC is synthesized not only by the mitochondrial pathway, but also by the vacuolar and the Kennedy pathways (23) (Fig. S1). Thus, we next addressed the growth of *gem1Δ* strains under conditions in which cells rely solely on mitochondrial synthesis. Toward this end, we impaired vacuolar PE synthesis by deleting the PS decarboxylase Psd2, and prevented PE biosynthesis through the Kennedy pathways by plating cells on medium devoid of ethanolamine and choline and deleting the dihydrosphingosine phosphate lyase Dpl1 (23) (Fig. S1). Under these conditions, *gem1Δ* cells demonstrated a dramatic growth defect (Fig. 3*D*, dashed box), indicating that mitochondrial de novo PC biosynthesis is affected by *GEM1* deletion. Interestingly, this growth defect was observed only on a nonfermentable carbon source (synthetic complete + glycerol, SCG) and could be partially rescued by the addition of exogenous ethanolamine, but not choline (Fig. 3*D*). This phenotype is reminiscent of that of *psd1Δ* cells, which likewise are auxotrophic for ethanolamine only on nonfermentable carbon sources (23). Taken together, these data indicate that Gem1-regulated ERMES activity may not be important in standard laboratory conditions, but might become important in more challenging conditions, such as when CL biosynthesis is compromised.

Gem1 is conserved in all main branches of the eukaryotic lineage, raising the intriguing possibility that Miro GTPases also function at ER–mitochondria connections in other clades. Mammals have two Miro GTPases, Miro-1 and Miro-2. We used a monoclonal antibody directed against hMiro-1 to localize Miro-1 in monkey fibroblastoid cells (COS-7 cells) by immunofluorescence. Mitochondria were visualized by MitoTracker staining (Fig. 4*A*, *Upper Left*) or an α-Tomm-20 antibody (Fig. S4*F*), and the ER network was visualized by a transfected ER marker, Sec61β-GFP (Fig. 4*A*, *Lower Left*). Miro-1 staining was observed in a few foci per mitochondria, strongly reminiscent of ERMES foci (Fig. 4*A*, *Upper Right* and Fig. S4*A*). Miro-1 foci consistently coincided with ER tubules (Fig. 4*B* and Fig. S4 *B–F*). This was particularly evident in images of mitochondria localized in the cell periphery, where most of the mitochondrial surface was resolvable from the ER. These data suggest that Miro GTPases are integral components of ER–mitochondria encounter structures in yeast and metazoans.

Discussion

ERMES-mediated ER–mitochondria connections lie at a crossroads of several biosynthetic pathways. ERMESs are important for interorganelle phospholipid exchange, they connect to the replicating mitochondrial genome, and they may influence the import of cytosolic proteins into mitochondria. Here we provide a hint that ERMESs are not passive, static structures but contain at least one regulatory component. Regulation of ERMES contact sites potentially could affect all of these processes.

Our study identified the Ca^{2+}-binding Miro GTPase Gem1 as an ERMES subunit. Gem1 is present in ERMES complexes in substoichiometric amounts and is not necessary for ERMES assembly, consistent with the idea that its role is regulatory rather than structural. Gem1 affects the size and number of ERMES foci in the cell and affects phospholipid homeostasis.

Gem1 contains four potential regulatory modules. These include two GTPases that, by analogy to other GTPases, are likely to be molecular switches responsive to input signals provided by GTPase-effector proteins, including nucleotide exchange factors (GEFs), GTPase-activating proteins (GAPs), and guanine nucleotide dissociation inhibitors (GDIs). Gem1 also contains two EF hands that likely are responsive to elevated Ca^{2+} concentrations.

Through mutagenesis, we have shown that these modules affect ERMES complexes in distinct ways and thus are experimentally separable. The first GTPase domain and the first Ca^{2+}-binding domain in Gem1 regulate Gem1 association with the ERMES complex, suggesting that these two domains are part of a regulatory circuit that converges on a common output. The GTPase and Ca^{2+}-binding modules could function either sequentially or in parallel as coincidence detectors. The physiological conditions that generate the appropriate input signals for Gem1 to associate with ERMES remain unknown.

The second GTPase domain is not involved in Gem1 localization to ERMES but influences ERMES activity. So far, no function can be attributed to Gem1's second Ca^{2+}-binding domain. Taken together, our results suggest that Gem1 cycles between a free state and an ERMES-bound state. Once bound to ERMES, it positively stimulates phospholipid exchange, requiring its second GTPase module in the process. The physiological conditions that generate the appropriate input signals for Gem1 to associate with ERMES and to modulate phospholipid transfer on and off remain unknown.

Gem1 may be controlling ERMES size to ensure that ERMES foci are made and undone at the right time and the right place to optimize resource utilization according to cellular needs. GTP may be used by Gem1 strictly for regulatory purposes, or it could

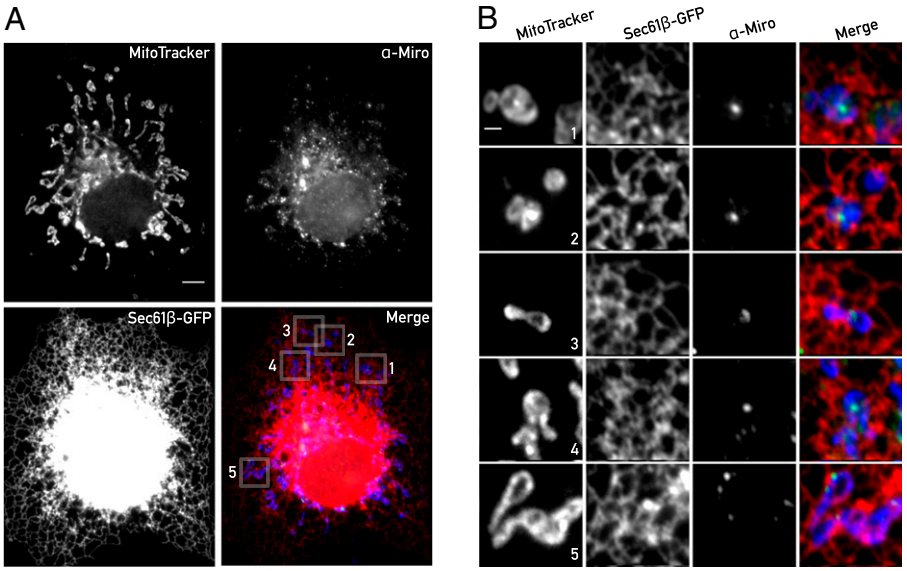

Fig. 4. (*A*) Miro-1 as detected by an α-Miro-1 antibody is found on ERMES-like foci (*Upper*, *Right*) on the mitochondrial surface (detected by MitoTracker-CMXRos staining; *Upper*, *Left*). The ER is labeled by Sec61β-GFP expression (*Lower*, *Left*). (Scale bar: 5 μm.) (*B*) Higher magnifications of the boxes in *A*. ERMES-like Miro-1 foci (green) coalign on both the mitochondrial (blue) and ER (red) networks. (Scale bar: 1 μm.)

provide the energy required for this task. The fact that Gem1 is not required for ERMES assembly per se might explain why Gem1 deletion has only a modest effect on steady-state mitochondrial phospholipid levels. In contrast, we showed that Gem1 function becomes essential under more demanding conditions, such as when cells have to cope with reduced CL content and are actively respiring.

Although numerous SMP-domain containing proteins in mammalian cells are candidates to serve as functional ERMES orthologs, none of them exhibits convincing structural homology outside these domains. In contrast, Miro proteins readily stand out as bona fide metazoan Gem1 orthologs that align over its entire length. Thus, Gem1 is the only ERMES constituent that can be unambiguously identified in metazoan cells. Indeed, our immunofluorescence analyses in mammalian fibroblasts show that Miro-1 is localized in discrete puncta, and these foci appear localized at ER–mitochondria interfaces, consistent with the possibility that Miro, like its yeast counterpart Gem1, plays a role in ER–mitochondria communication.

Such a hypothetical function for Miro would be different from its previously described role as an adapter between mitochondria and the microtubule cytoskeleton, thought to regulate mitochondrial movement in a Ca^{2+}-dependent manner (12, 13). It has recently been proposed that ER and mitochondrial dynamics occur on a subset of microtubules that are posttranslationally modified by acetylation (24). Finding both ER and mitochondria on the same cellular routes may be important to promoting their encounter, perhaps reconciling the two proposed functions of Miro.

Our finding that metazoan Miro localizes to ER–mitochondria contact sites sheds a different light on the previous finding that Miro overexpression leads to increased Ca^{2+} uptake by mitochondria upon ER store depletion (25). This phenomenon was attributed to an indirect effect of mitochondrial redistribution within the cells. Our findings hint at a potentially more direct role of Miro in organizing microdomains, where Ca^{2+} movement could be facilitated at ER–mitochondria contact sites. The results may explain the elevated level of apoptosis in cells overexpressing mutant forms of Miro as a result of increased Ca^{2+} transfer between the ER and mitochondria (26). It is interesting to note that the measured affinity of Miro for Ca^{2+} is low (K_d ~50 μM) (13), making it attractive to speculate that the molecular environment at the junctions might allow for sufficiently high local Ca^{2+} concentrations to allow saturation of Miro/Gem1 Ca^{2+}-binding sites (27).

Miro was recently proposed to interact with Mitofusin (Mfn) 1 and 2, and Mfn-2 was shown to be required for Miro-dependent mitochondrial movement along axons (28). Mfn-2 also has been described as a potential tether between the ER and mitochondria in mammalian cells (29). A dual function of Miro in mitochondrial motility and ER tethering might help reconcile the dual function of Mfn-2 in the same processes.

Materials and Methods

Yeast Culture and Transformation. All yeast transformations were done using standard methods. Loci replacements were achieved using the Pringle PCR toolbox (30).

Purification of ERMES Complexes. Yeast strains bearing a C-terminal TAP tag on either Mmm1 or Mdm34 (30) were grown in YP medium containing 3% glycerol and 3% ethanol to an OD of 1–1.5. Between 4,000 and 8,000 OD were routinely harvested, washed three times in homogenization buffer [20 mM Hepes-KOH (pH 7.4), 150 mM potassium acetate, 2 mM magnesium acetate, 10% glycerol, 1 mM EGTA, 1 mM DTT, Complete Protease Inhibitor (Roche)] and resuspended in 1 volume of the same buffer. Cells were frozen by dripping into liquid nitrogen and cryomilled with a Retsch MM-301 mixer mill (5× 3 min at 12 Hz). The powder was then thawed on ice, and digitonin was added to a final concentration of 2% from a 10% stock solution. Membrane solubilization was allowed to occur for 60 min at 4 °C with rotation. Cell debris was spun down for 15 min at 12,000 × *g*. Then 6×10^7 pre-equilibrated IgG-coated epoxy Dynabeads (M-270; Invitrogen) were added to the cell extract. IgG coupling was performed according to the manufacturer's protocol. Complexes were allowed to bind to the beads for 2 h at 4 °C. Beads were then separated with a magnet and washed six times for 3 min in 1 mL of homogenization buffer. Complexes were released from beads by tag cleavage with 1 μL of AcTEV (Invitrogen) for 20 min at 14 °C in 30 μL total volume. AcTEV was then selectively removed by incubation with 15 μL of prequilibrated Dynabeads (TALON; Invitrogen) for 15 min at 4 °C.

Complexes were resolved by SDS/PAGE and stained by silver staining or colloidal Coomassie blue and processed for liquid chromatography–tandem mass spectrometry for peptide identification at the University of California San Francisco mass spectrometry facility.

Live Microscopy. Cells expressing a N-terminal mCherry-tagged Mdm34 from its own locus (4) and a C-terminal 2× Flag-GFP–tagged Gem1 on a centromeric plasmid were cultured in synthetic complete medium with ethanol and glycerol as sole carbon source. After being transferred to imaging

coverslips, cells were imaged with a Yokogawa CSU22 Spinning Disk confocal mounted on a Nikon Eclipse Ti-E inverted microscope equipped with a 100×/1.40-na oil Plan Apo VC objective. GFP was excited with a 491-nm cobalt laser, and mCherry was excited with a 456-nm solid-state laser. A Photometrics Evolve EM CCD camera was used for acquisition. Automation was performed using μManager software. Image processing was done using ImageJ software. The amount of GFP-Gem1 signal colocalizing with Mdm34-mCherry was determined by dividing the amount of Gem1 found in ERMES foci by the total area of ERMES foci. These two parameters were acquired automatically using ImageJ Script S1 (*SI Appendix*). Images in Fig. 1*C* were acquired on the OMX microscope and subjected to denoising and deconvolution as described previously (31).

ERMES Size Quantification. Cells expressing a N-terminal Mdm34-GFP fusion protein (4) were imaged as above except with medium containing 3% glucose as a carbon source. Z series (0.4 μm) were acquired in the bright-field and GFP channels. The images were then processed with ImageJ Script S2 (*SI Appendix*). Five images containing 60 cells on average were processed for each genotype.

Immunofluorescence. Cos-7 cells were cultured in DMEM supplemented with 10% FCS, glutamine, penicillin, and streptomycin. Cells were seeded on acid-washed glass coverslips in 35-mm dishes and transfected with 3 μL of Fugene 6 (Roche) and 2 μg of Sec-61β-GFP plasmid (24) according to the manufacturer's protocol. On the next day, slides were optionally stained with 2 mM MitoTracker Red CM-H_2XRos (Invitrogen), washed in PBS, fixed in 6% paraformaldehyde in PHEM buffer [60 mM Pipes (pH 6.9), 25 mM Hepes, 10 mM EGTA, 2 mM $MgCl_2$] for 15 min at 20 °C. Slides were then washed three times for 5 min each in PHEM plus 0.1% Triton-X100 and blocked with 100% goat serum (Invitrogen). Incubation with the primary antibodies was done in goat serum for 2–4 h. Antibody concentrations were as follows: anti–Miro-1, mouse monoclonal (4H4; Sigma-Aldrich), 0.2 μg/mL; anti–α-Tomm-20, rabbit polyclonal (ab78547, Abcam), 1.5 μg/mL.

Slides were washed four times for 5 min each with PHEM plus 0.1% Triton-X100. Secondary antibody incubation were done with Alexa Fluor 350–, Alexa Fluor 405–, Alexa Fluor 488–, Alexa Fluor 546–, or Alexa Fluor 633–conjugated goat anti-mouse or anti-rabbit antibodies (Invitrogen) in 100% goat serum at a final concentration of 4 μg/mL for 1–2 h. After four 5-min washes in PHEM plus 0.1% Triton-X100, slides were mounted in fluorescence mounting medium (Dako) and sealed with nail polish. Slides were imaged on a Zeiss Axiovert 200M fluorescence microscope. GFP and Alexa Fluor 488 were imaged using an FITC filter set (Filter Set 38; Zeiss), MitoTracker Red and Alexa Fluor 546 were imaged using a Texas Red filter set (Filter Set 45), and Alexa Fluor 350 and Alexa Fluor 405 were imaged using a modified DAPI filter set (Filter Set 01), in which the low-pass emission filter was replaced by a D445/50m bandpass filter (Chroma Technology).

ACKNOWLEDGMENTS. We thank all members of the P.W. laboratory for stimulating discussions. We are grateful to M. Cronin and T. L. Schwarz for the generous gift of plasmids and helpful discussions, the University of California San Francisco mass spectrometry facility, especially H. Hernández-Barry, for mass spectrometry analysis, and J. Sedat and J. Fung for invaluable help with the OMX microscope. B.K. and C.O. are fellows of the Swiss National Science Foundation and the German Research Foundation, respectively. P.W. is an investigator of the Howard Hughes Medical Institute.

1. Pizzo P, Pozzan T (2007) Mitochondria–endoplasmic reticulum choreography: Structure and signaling dynamics. *Trends Cell Biol* 17:511–517.
2. Levine T, Loewen C (2006) Inter-organelle membrane contact sites: Through a glass, darkly. *Curr Opin Cell Biol* 18:371–378.
3. Kornmann B, Walter P (2010) ERMES-mediated ER–mitochondria contacts: Molecular hubs for the regulation of mitochondrial biology. *J Cell Sci* 123:1389–1393.
4. Kornmann B, et al. (2009) An ER–mitochondria tethering complex revealed by a synthetic biology screen. *Science* 325:477–481.
5. Kopec KO, Alva V, Lupas AN (2010) Homology of SMP domains to the TULIP superfamily of lipid-binding proteins provides a structural basis for lipid exchange between ER and mitochondria. *Bioinformatics* 26:1927–1931.
6. Hobbs AE, Srinivasan M, McCaffery JM, Jensen RE (2001) Mmm1p, a mitochondrial outer membrane protein, is connected to mitochondrial DNA (mtDNA) nucleoids and required for mtDNA stability. *J Cell Biol* 152:401–410.
7. Meeusen S, Nunnari J (2003) Evidence for a two-membrane–spanning autonomous mitochondrial DNA replisome. *J Cell Biol* 163:503–510.
8. Meisinger C, et al. (2004) The mitochondrial morphology protein Mdm10 functions in assembly of the preprotein translocase of the outer membrane. *Dev Cell* 7:61–71.
9. Boldogh IR, et al. (2003) A protein complex containing Mdm10p, Mdm12p, and Mmm1p links mitochondrial membranes and DNA to the cytoskeleton-based segregation machinery. *Mol Biol Cell* 14:4618–4627.
10. Jaffe AB, Hall A (2005) Rho GTPases: Biochemistry and biology. *Annu Rev Cell Dev Biol* 21:247–269.
11. Youngman MJ, Hobbs AEA, Burgess SM, Srinivasan M, Jensen RE (2004) Mmm2p, a mitochondrial outer membrane protein required for yeast mitochondrial shape and maintenance of mtDNA nucleoids. *J Cell Biol* 164:677–688.
12. Guo X, et al. (2005) The GTPase dMiro is required for axonal transport of mitochondria to *Drosophila* synapses. *Neuron* 47:379–393.
13. Wang X, Schwarz TL (2009) The mechanism of Ca^{2+}-dependent regulation of kinesin-mediated mitochondrial motility. *Cell* 136:163–174.
14. Frederick RL, McCaffery JM, Cunningham KW, Okamoto K, Shaw JM (2004) Yeast Miro GTPase, Gem1p, regulates mitochondrial morphology via a novel pathway. *J Cell Biol* 167:87–98.
15. Frederick RL, Okamoto K, Shaw JM (2008) Multiple pathways influence mitochondrial inheritance in budding yeast. *Genetics* 178:825–837.
16. Koshiba T, et al. (2011) Structure-function analysis of the yeast mitochondrial Rho GTPase, Gem1p: Implications for mitochondrial inheritance. *J Biol Chem* 286:354–362.
17. Sigal IS, et al. (1986) Mutant ras-encoded proteins with altered nucleotide binding exert dominant biological effects. *Proc Natl Acad Sci USA* 83:952–956.
18. Feig LA, Cooper GM (1988) Inhibition of NIH 3T3 cell proliferation by a mutant ras protein with preferential affinity for GDP. *Mol Cell Biol* 8:3235–3243.
19. Calés C, Hancock JF, Marshall CJ, Hall A (1988) The cytoplasmic protein GAP is implicated as the target for regulation by the ras gene product. *Nature* 332:548–551.
20. Osman C, Haag M, Wieland FT, Brügger B, Langer T (2010) A mitochondrial phosphatase required for cardiolipin biosynthesis: The PGP phosphatase Gep4. *EMBO J* 29:1976–1987.
21. Kuroda T, et al. (2011) FMP30 is required for the maintenance of a normal cardiolipin level and mitochondrial morphology in the absence of mitochondrial phosphatidylethanolamine synthesis. *Mol Microbiol* 80:248–265.
22. Gohil VM, Thompson MN, Greenberg ML (2005) Synthetic lethal interaction of the mitochondrial phosphatidylethanolamine and cardiolipin biosynthetic pathways in *Saccharomyces cerevisiae*. *J Biol Chem* 280:35410–35416.
23. Birner R, Bürgermeister M, Schneiter R, Daum G (2001) Roles of phosphatidylethanolamine and of its several biosynthetic pathways in *Saccharomyces cerevisiae*. *Mol Biol Cell* 12:997–1007.
24. Friedman JR, Webster BM, Mastronarde DN, Verhey KJ, Voeltz GK (2010) ER sliding dynamics and ER–mitochondrial contacts occur on acetylated microtubules. *J Cell Biol* 190:363–375.
25. Saotome M, et al. (2008) Bidirectional $Ca2^{+}$-dependent control of mitochondrial dynamics by the Miro GTPase. *Proc Natl Acad Sci USA* 105:20728–20733.
26. Fransson A, Ruusala A, Aspenström P (2003) Atypical Rho GTPases have roles in mitochondrial homeostasis and apoptosis. *J Biol Chem* 278:6495–6502.
27. Csordás G, et al. (2010) Imaging interorganelle contacts and local calcium dynamics at the ER–mitochondrial interface. *Mol Cell* 39:121–132.
28. Misko A, Jiang S, Wegorzewska I, Milbrandt J, Baloh RH (2010) Mitofusin 2 is necessary for transport of axonal mitochondria and interacts with the Miro/Milton complex. *J Neurosci* 30:4232–4240.
29. de Brito OM, Scorrano L (2008) Mitofusin 2 tethers endoplasmic reticulum to mitochondria. *Nature* 456:605–610.
30. Longtine MS, et al. (1998) Additional modules for versatile and economical PCR-based gene deletion and modification in *Saccharomyces cerevisiae*. *Yeast* 14:953–961.
31. Carlton PM, et al. (2010) Fast live simultaneous multiwavelength four-dimensional optical microscopy. *Proc Natl Acad Sci USA* 107:16016–16022.

Script S1

```
//Open micromanager file, convert it to two individual images for GFP
and mCherry channels :

run(" Open Micro-Manager File");
rename("dd");
run(" Copy to Stacks (channels)");
selectWindow("dd_BF");
close();
selectWindow("dd");
close();

//Subtract backround on the GFP channel :

selectWindow("dd_GFP-100%");
run("Subtract...", "value=1000");

//determine position of ERMES foci by thresholding the Mdm34-mCherry
image and particle analysis, which removes large particles likely
representing autofluorescent vacuoles :

selectWindow("dd_mCherry-80%");
setThreshold(5696, 43324);
run("Analyze Particles...", "size=2-20 pixel circularity=0.80-1.00
show=Masks");

//measure the total area of ERMES foci :
selectWindow("Mask of dd_mCherry-80%");
run("Measure");

//measure the amount GFP-Gem1 in ERMES foci :
run("Image Calculator...", "image1=dd_GFP-100% operation=Multiply
image2=[Mask of dd_mCherry-80%] create 32-bit");
run("Measure");

//close all images :
selectWindow("dd_GFP-100%");
close();
selectWindow("dd_mCherry-80%");
close();
selectWindow("Mask of dd_mCherry-80%");
close();
close();
```

Script S2

```
//open MicroManager file, rename it

run(" Open Micro-Manager File");

rename("input");

//make z-projection, convert to individual images for BF and GFP
channels

run(" Z Project", "start=1 stop=11 projection=[Max Intensity] output");

selectWindow("input");

close();

run(" Copy to Stacks (channels)");
```

```
selectWindow("input Projection");
close();


//reduce noise by applying a gaussian blur, apply threshold and run a
particle analysis to detect and count ERMES foci
selectWindow("input Projection_GFP-100%");
run("Gaussian Blur...", "sigma=2");
setThreshold(1000, 65890);
run("Analyze Particles...", "size=0.030-3.0 circularity=0.5-1.00
show=Nothing display exclude clear summarize add");
//copy result for analysis in spreadsheet program
String.copyResults();
```

Supporting Information

Kornmann et al. 10.1073/pnas.1111314108

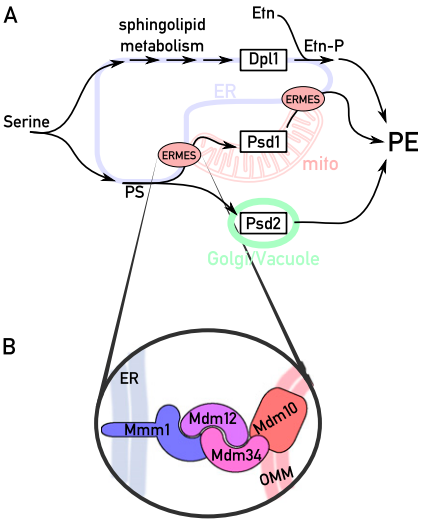

Fig. S1. (*A*) Biosynthetic pathways of PE. PE can be synthesized from different pathways. First, serine is incorporated into PS. PS is decarboxylated by both PS decarboxylases Psd1 and Psd2, in the mitochondria and in the Golgi/vacuole, respectively. A third pathway involves sphingolipid metabolism. Dpl1 is a dihydrosphingosine phosphate lyase that degrades long-chain bases and produces ethanolamine-phosphate. This ethanolamine-phosphate or exogenously added ethanolamine can be incorporated into PE via the Kennedy pathways. The Psd1-dependent pathway relies on interorganelle phospholipid exchange facilitated by ERMES. (*B*) Schematic of the ERMES complex. Mdm10 is a β-barrel protein inserted in the OMM. Mmm1 is an ER integral protein. Mmm1, Mdm12, and Mdm34 are structurally related. The transmembrane topology of individual components has been experimentally established, but the pattern of pairwise interactions is hypothetical.

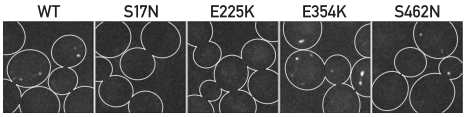

Fig. S2. Indicated mutants of Gem1 were expressed as N-terminal 2× Flag-GFP fusions under the Gem1 promoter in cells bearing a deletion of the endogenous *GEM1*. Imaging was performed as in Fig. 2*D*.

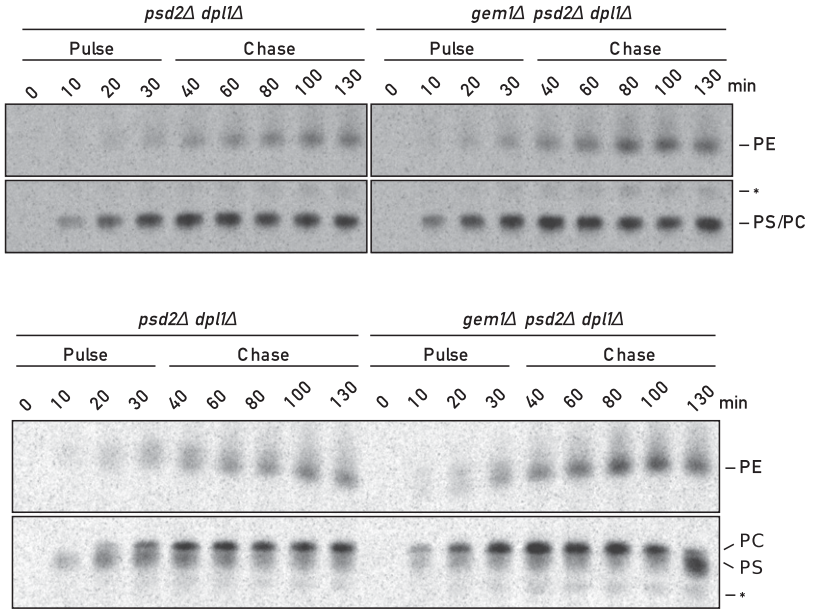

Fig. S3. Kinetic of PE accumulation after a pulse-chase with ^{14}C-serine. Total cellular lipids were extracted at the indicated time points of the pulse or the chase phase and subjected to TLC to measure label incorporation in the indicated phospholipid species. No significant difference was observed in the rate of PE synthesis between the Gem1-proficient and Gem1-deficient cells. (*Lower*) A repetition of the first experiment with different TLC conditions that allow a better separation of PS and PC.

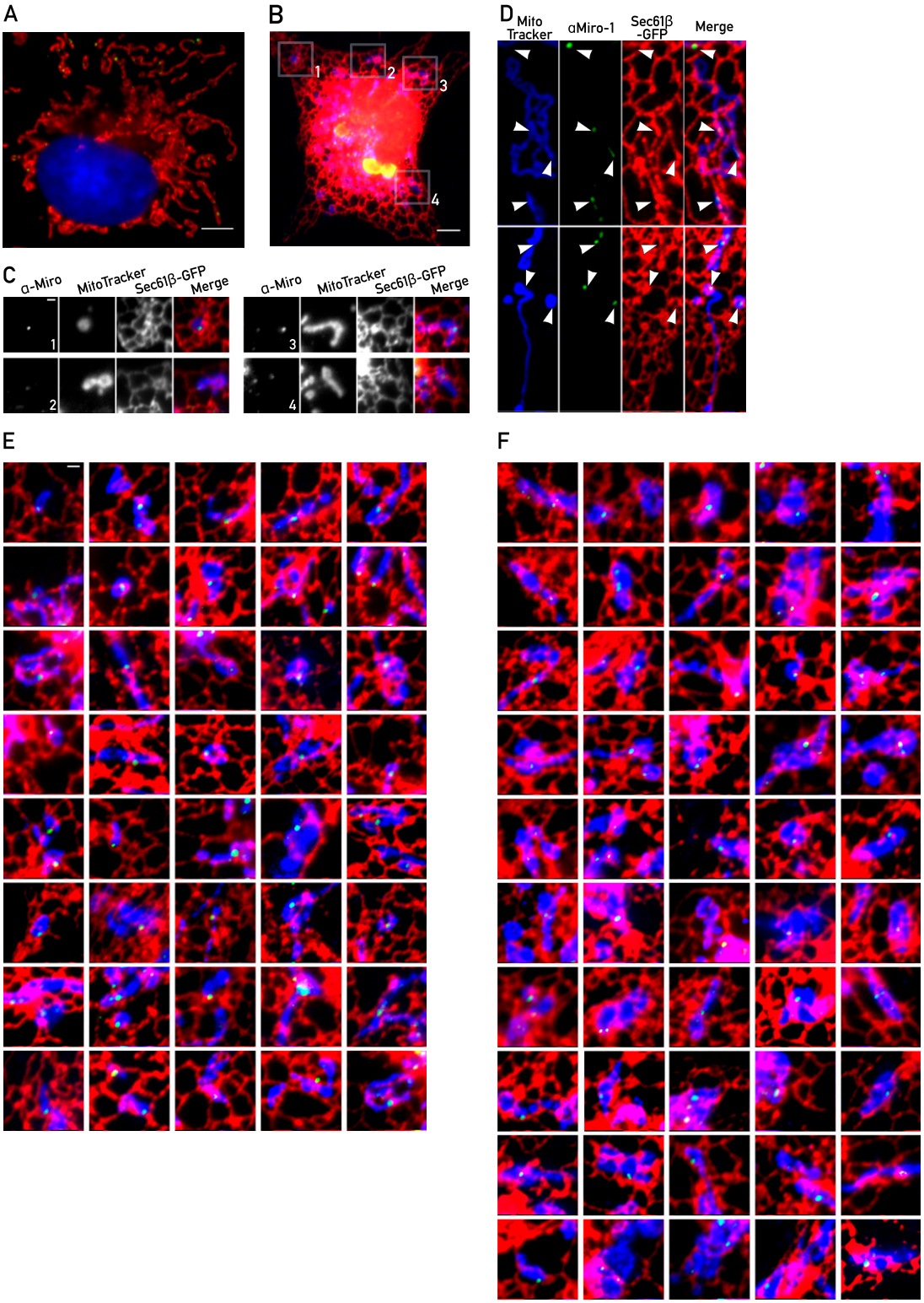

Fig. S4. (*A*) Miro staining in foci is not an artifact of Sec61β-GFP expression, because the same can be observed in nontransfected cells (blue, DAPI staining; red, MitoTracker staining; green, α-Miro1 staining). (Scale bar: 5 μm.) (*B*) Another cell processed as in Fig. 4 (blue, MitoTracker staining; red, Sec61β-GFP staining; green, α-Miro1 staining). (Scale bar: 5 μm.) (*C*) Higher magnifications of the boxes in *B*. (Scale bar: 1 μm.) (*D*) Confocal images obtained with the same experimental setup as in Fig. 4. (*E*) More examples of highly magnified cells processed as in Fig. 4*B* (blue, MitoTracker staining; red, Sec61β-GFP staining; green, α-Miro1 staining). (Scale bar: 1 μm.) (*F*) As in *E*, except that MitoTracker was omitted, and mitochondria were detected by an antibody against the outer membrane protein α-Tomm-20 (blue, α-Tomm-20 staining; red, Sec61β-GFP staining; green, α-Miro1 staining). (Scale bar: 1 μm.)

Other Supporting Information Files

SI Appendix (PDF)